AIChE

Condensed Rotational Separation of CO_2 from Natural Gas

G. P. Willems
Div. of Thermo Fluids Engineering, Dept. of Mechanical Engineering, 5600 MB Eindhoven, The Netherlands

M. Golombok
Div. of Thermo Fluids Engineering, Dept. of Mechanical Engineering, 5600 MB Eindhoven, The Netherlands, and
Shell Exploration and Production bv, P.O. Box 60, 2280 AB Rijswijk, The Netherlands

G. Tesselaar
Shell Global Solutions bv, P.O. Box 60, 2280 AB Rijswijk, The Netherlands

J. J. H. Brouwers
Div. of Thermo Fluids Engineering, Dept. of Mechanical Engineering, 5600 MB Eindhoven, The Netherlands

DOI 10.1002/aic.11995
Published online August 24, 2009 in Wiley InterScience (www.interscience.wiley.com)

This article describes measurements of methane purification by condensed rotational separation. First, the separation concept is introduced. Then the test-setup and measurements are described. The thermodynamic performance of the system is compared with thermodynamic predictions and is found to be in good agreement. The separation performance *of the centrifugal separator is addressed.* © 2009 American Institute of Chemical Engineers *AIChE J,* 56: 150–159, 2010
Keywords: separation techniques, Phase equilibrium, Condensation, gas purification, demisting

Introduction

A steadily increasing fraction of newly located natural gas reserves is severely contaminated with CO_2 and H_2S. Fields containing large fractions of contaminants cannot be economically produced with currently available technology, predominantly based on amine solvent treaters.[1] The applicable pipeline specification means that the gas has to be produced containing a maximum of 2–3% CO_2.[1,2] This is reachable by amine treatment, however, this treatment is not economically feasible for heavily contaminated gas because of the associated high solvent regeneration costs. Thus, there is a need to develop gas cleaning methods that can cope with high contamination levels up to 70 mol% H_2S and/or CO_2.[3] One of these new methods is called C3sep, Condensed Contaminant Centrifugal Separation.[4] We have previously described the process mechanisms, the underlying physical concepts, and the design of a small scale prototype.[5] In addition to ''upstream'' applications, for purifying natural gas, the technique also has potential for removing CO_2 from combustion effluent and CO_2 from syngas.

The technology works by expanding, and simultaneously uniformly cooling, a high pressure contaminated gas, which results in small liquid droplets, homogeneously dispersed, within the gas stream. For natural gas applications, these droplets are enriched in contaminants typically CO_2 and H_2S.[6] The output gas stream is therefore enriched in methane and depleted in contaminants. When in equilibrium, these droplets grow slowly by coagulation and have to be spatially separated from the purified product gas. This separation can be done by several techniques. Depending on the size of droplets that can be collected, the required growth

Correspondence concerning this article should be addressed to M. Golombok at michael.golombok@shell.com

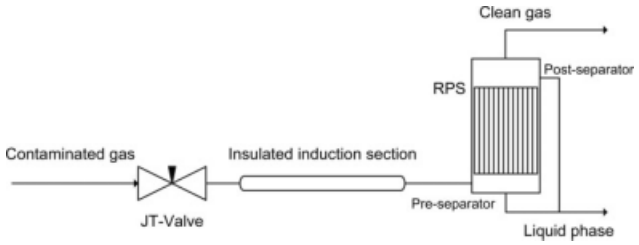

Figure 1. Core separation process.

time varies. A waiting time of ~100 s has to be observed to wait until the droplets have reached a size of about 20 μm,[5] which is a size that can be efficiently separated with a cyclone separator.[7] At high gas flow rates, this results in very large equipment. Because of the cryogenic temperatures and high pressures, the corresponding investments would be huge. When the growth time can be limited, the equipment size would diminish. At high gas flow rates (ca. 300 MMscf/d $\approx$ 360.000 nm^3/h), a residence time less than 1s is advisable to keep capital costs low. To achieve such short residence times, a separation technology is required that can collect micron-sized droplets, which is not possible with state of the art rotating technology.

In our new process, the spatial separation of the two phases is done by a rotating particle separator (RPS), which uses a large centrifugal force in combination with small (1 mm) channels to separate small droplets within very short residence times.[8–13] The contaminants, i.e., CO_2 and H_2S in the waste stream are in the liquid phase, which is ideal for storage or enhanced oil recovery purposes. C3sep is a bulk separation process, i.e., it can economically separate large amounts of CO_2 and H_2S from methane. Because the droplets are in thermodynamic equilibrium with the gas, no complete separation of the gases can be achieved, even when the phases are separated completely. The droplets will still contain traces of CH_4 and the gas will still contain CO_2. Therefore, the cleaned gas needs treatment with other technology, such as amine treatment, to reach the purity that is required for grid applications, i.e., the 2–3% CO_2 mentioned earlier. Depending on the concentration of the contaminated gas and operation conditions of the process, a methane purity of 83–99 mol% can be achieved, with C3sep.

This study focuses on the measurements performed on the first prototype described by van Wissen.[5] In the next section, we describe the process and the experimental setup, followed by the separation of the condensed phase and discussion in the subsequent sections.

Process Background

The C3sep process background incorporates expansion cooling, formation, and growth of droplets rich in the contaminating substance and subsequent separation of these droplets, see Figure 1.

The contaminated gas at high pressure is expanded, e.g., with a Joule Thomson(JT)-valve. The gas then cools down because of the expansion and the contaminants preferentially condense into a mist of droplets. The droplets get time to grow while passing the insulated induction section. The droplets of a few μm are subsequently separated with the rotational particle separator.

Thermodynamics

Because of the binary condensation, a mist of small droplets is formed, which quickly reaches thermodynamic equilibrium. The droplets will then only grow because of coagulation, which is a process that relies on the mobility of the droplets. When droplets grow, the mobility rapidly decreases.[14] Overall this results in micron-sized droplets when a growth time of ~1 s is present. To separate these micron-sized droplets, a special centrifugal separation device is required, the RPS.

The liquid phase will mostly contain molecules of the species with the lowest partial vapor pressure.[7] The vapor phase will mainly contain molecules of the species with the highest partial vapor pressure. The two phases, liquid and vapor phase, finally end up in equilibrium. The concentration depends on pressure, temperature, and start composition. A phase separator as schematically depicted in Figure 2 is used to separate the vapor and liquid phase. The multiphase feed (z) enters the phase separator and is divided into a equilibrium gaseous (y) and a liquid fraction (x).

The (methane) enrichment is the change in mole fraction (methane) between feed (z) and product (y) stream. The enrichments is therefore an important parameter to define the performance of the separation system for it determines the purity of the product. The ratio between the number of moles of methane in the product stream and the number of moles of methane in the feed stream is called recovery and can be defined as[5]:

$$r_1 = \frac{y_1 Q_P}{z_1 Q_F} = \frac{y_1(z_1 - x_1)}{z_1(y_1 - x_1)} \tag{1}$$

where Q is the mole flow rate, with F and P denoting feed and product gas, respectively. x_i,y_i, and z_i are the mole fraction of component i in the liquid waste, product, and feed, where $i = 1$ refers to methane. With the described process, we can choose between high recoveries and low enrichments or high enrichments at the expense of a lower recovery rate (y_1 vs. r_1). Normally the higher the pressure the higher the enrichment but at the expense of a lower recovery rate, i.e., because more methane will dissolve in the liquid CO_2. With pure CO_2 and CH_4 mixtures it is difficult, because of the thermodynamic

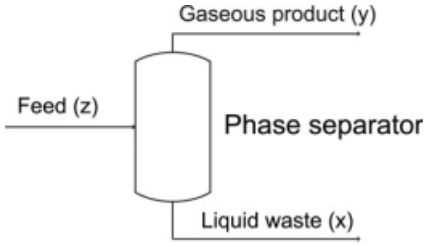

Figure 2. Schematic phase separation, an equilibrium multi phase stream is divided into a gaseous and liquid stream.

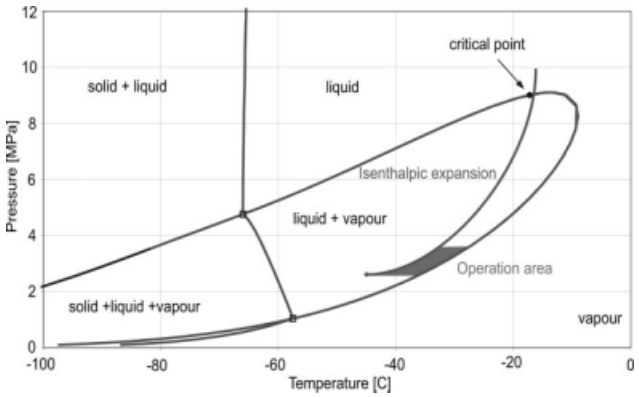

Figure 3. Phase diagram corresponding to CH_4(1) + CO_2(2): $z_1 = 0.5$.

An extended equation of state program based on a cubic equation of state of the Soave-Redlich-Kwong type with pure component parameters fitted to vapor pressures and liquid densities along with a composition dependent mixing rule is used. A freeze out model $T < T_{solid}$ CO_2 is incorporated. In the lower right corner, the operation area of our setup is indicated.

properties, to reach concentrations exceeding 85 mol% CH_4.[1] When H_2S is present in the natural gas, the freeze out temperature of the CO_2 shifts to lower temperatures, thereby unleashing possible enrichment up to gas concentrations over 95 mol% at high recovery rates.[5]

Van Wissen[5] has optimized the operating pressure and temperature for binary mixtures (CH_4/CO_2) as a function of three recovery values, i.e., $r_1 = 0.9$, $r_1 = 0.95$, and $r_1 = 0.98$. In general, the lower the pressure at constant temperature, the higher the recovery of methane, but the enrichment diminishes due to the high amounts of CO_2 that do not condense. The optimal pressures and temperatures can be found in the lower left corner of the "liquid and vapor" phase, close to the freeze out curve (the vertical line at -60°C in Figure 3). The optimal and most economical process conditions for real applications have to be determined while incorporating the whole gas treatment facility in the analysis.

In our experiments, we use a binary mixture of methane (CH_4) and carbon dioxide (CO_2) with a mole fraction of methane ranging from $z_1 = 0.2$ to $z_1 = 0.8$. The phase diagram of the mixture varies considerably with the the concentration. A typical phase diagram corresponding to a mixture fraction of $z_1 = 0.5$ can be found in Figure 3.

When the mixture is expanded from the gas phase to a pressure and temperature within the liquid and vapor regime, small liquid droplets are formed. The concentration of each phase as well as several other properties of both phases can be calculated using isothermal flash calculations. The line on the lower right side of the phase diagram, dividing the liquid and vapor and vapor area is called the dew-pointing line.

Separation

One of the key features of the test setup is the novel phase separator, which has been described by van Wissen.[5] This phase separator is designed to separate large amounts of liquid CO_2 droplets larger then 1 μm from a semi-cryogenic (-60°C) natural gas stream. The separator consists out of a preseparator, a coagulation element, and a postseparator section. A number of aspects concerning the separator performance are now described.

Preseparator Performance. The rotating particle separator is constructed with an integrated cyclone, as a preseparator. The preseparator is constructed with a tangential inlet to provide the rotating flow. To calculate the efficiency of this preseparator, we first look at the efficiency of a gravitational separator. In case of a gravitational separator, the terminal settling velocity (v_T) of the particle is used, i.e., the velocity of the particle when drive and drag force are in equilibrium, to predict the performance. The v_T for a small particle where viscous forces are dominating (a so called Stokes particle) is described by[15]:

$$v_T = \frac{(\rho_p - \rho_g) d_p^2 g}{18\mu} \tag{2}$$

with ρ_p, the density of the particle/droplet; ρ_g the density of the gas; d_p the diameter of the particle/droplet; g, the gravitational acceleration; and μ, the dynamic viscosity of the fluid.

The particle diameter that this cyclone can collect with a 50% probability is called $d_{p50\%}$, and is analogous to the also used $d_{p100\%}$ which is the droplet size that is collected with a 100% probability. The $d_{p50\%}$ can be calculated with a relation based on the v_T of a particle under influence of a centrifugal force[5]:

$$d_{p50\%} = \sqrt{\frac{9\mu v_{ax}(r_w^2 - r_{50\%}^2)}{(\rho_p - \rho_g)\int_0^L v_t^2 dz}} \tag{3}$$

with v_{ax} the gas velocity in axial direction; v_t, the gas velocity in tangential direction; r_w, the radius of the wall; $r_{50\%}$ the radius half way between the inner and outer wall of the cyclone volute; and L, the length of the separator. The centrifugal acceleration has been described by v_t^2/r. The tangential velocity is assumed constant within the whole preseparator, because of the stabilizing influence of the rotating barrel. The velocity at the inside of the cyclone is equal to the barrel velocity, Eqn. 3 results in:

$$d_{p50\%} = \sqrt{\frac{9\mu v_{ax}(r_w^2 - r_{50\%}^2)}{(\rho_p - \rho_g) v_t^2 L}} \tag{4}$$

this yields a $d_{p50\%}$, which varies between 1 and 3.3 μm depending on the tangential speed of the separator element and gas flow rate. We use the $d_{p50\%}$ definition instead of the $d_{p100\%}$ definition because the turbulent flow will interfere with the particle collection.[16] As a result of turbulence, it is hard to define an efficiency of 100%, due to the fact that a small fraction of the droplets theoretically will never reach the wall. From Direct Numerical Simulation (DNS) calculations,[17] it follows that to achieve 98% separation efficiency the mono disperse particle diameter d_p should be around $3d_{p50\%}$ or the $d_{p50\%}$ should be chosen 1/3 d_p.

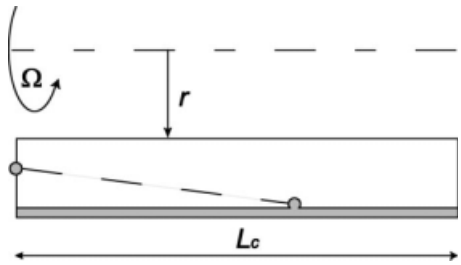

Figure 4. Droplet migration within a single RPS channel.

Separator Performance. For a single row of RPS channels or for a RPS constructed with a single row of channels (see Figure 7 below), a relation for the $d_{p50\%}$ of the channels can be derived with help of the v_T (see Figure 4).

In the figure, a single channel is depicted rotating around a central axis at a radius r. A droplet that enters the channel on the left side is forced to the outer wall of the channel with a velocity equal to the v_T. The distance the droplet has to travel to achieve 50% separation equals the radius of the channel, therefore in that case:

$$v_T \frac{L_c}{v_{ax}} = \frac{1}{2} d_c \tag{5}$$

where L_c is the length of the channels and d_c is the width of the channels. This can be rewritten:

$$d_{p50\%} = \sqrt{\frac{9 d_c \mu v_{ax}}{(\rho_p - \rho_g)\Omega^2 r L_c}} \tag{6}$$

where $\Omega^2 r$ is the magnitude of the centrifugal acceleration with Ω the rotational speed of the element (rad/s). The $d_{p50\%}$ varies between 0.3 and 1.2 μm depending on the rotational speed of the separator. Summarizing, the preseparator collects droplets from 1 to 3.3 μm upward and the coagulation element collects droplets as small as 0.3–1.2 μm.

Additional separation at stationary conditions is caused by the impactor effect because of the small space between the rotating element and housing at the entrance of the separator, which will be shown later. This impactor effect results in good separation efficiencies even at static conditions.

Experimental Setup

For testing, we have constructed a closed gas loop (60 nm^3/h) with a gas conditioning section and a separation section. For reference to industrial scales, this is equivalent to 50 ksf/d for a flow of 50/50 v/v CH_4/CO_2. The gas conditioning section simulates a gas well at variable composition (20–80 mol% CH_4 in CO_2) and pressures (above 8 MPa). The conditioned gas (60 nm^3/h) is fed to the separation section. In the separation section, the core process is located, which consists of the following.

- JT-valve, which expands and cools the gas.
- Induction section where droplets get time to nucleate and grow until the droplets eventually reach a size of a few microns.

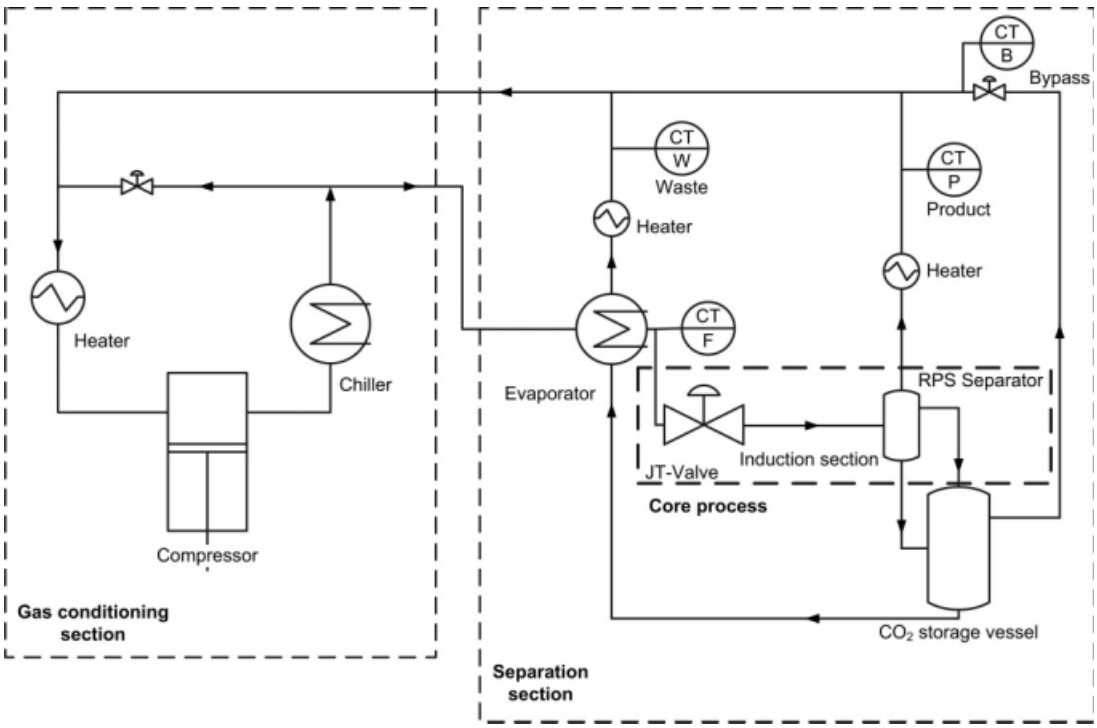

Figure 5. Schematic process layout, on the left side the gas condition section and on the right side the separation section.

The position of the concentration transmitters (CT) have been indicated by the circles with CT in the upper half of the circle.

• Rotating particle separator, which is a centrifugal separator with a bundle of axially orientated channels rotating around a common axis to separate the small waste droplets from the product gas.

The actual separation process is a once through process (see Figure 1). In Figure 5, an overview of the test loop layout can be found. On the left side of the figure, the gas conditioning section, which simulates a gas well is displayed. On the right side, the gas separation section comprising the core process can be found.

Gas conditioning section

The gas conditioning section is designed to cope with pressures up to 15 MPa, which is on the order of the surface manifold facility pressure of a gas treatment plant.[6] A diaphragm compressor (60 nm^3/h) recompresses the gas after it has been mixed to pressures up to 15 MPa. In the gas conditioning section, the gas is reconditioned to represent a real contaminated gas field. At startup, the gas is supplied to the suction side of the diaphragm compressor from premixed methane/carbon dioxide (e.g., 50 mol%/50 mol%) pressurised gas bottles via a pressure regulator. The concentration can be fine-tuned using bottles of pure methane and carbon dioxide. The gas should be delivered to the separation section at a pressure exceeding 10 MPa and a temperature around 20°C. These conditions are necessary to get to the right separation conditions after the expansion. After the gas is compressed, it is cooled by a tap water chiller to around ambient temperature to remove the heat added by the compression. The conditioned gas is sent to the separation section.

Separation section

The separation section of the test loop is constructed within an autoclave testing bunker and consists out of an evaporator/cooler, a Joule Thomson(JT)-valve, an induction section, the RPS, a liquid carbon dioxide collection vessel, a couple of heaters, and measuring equipment for pressures, temperatures, and concentrations in the induction section (see Figure 5).

The high pressure gas is first cooled in the evaporator with help of previously separated liquid carbon dioxide to ~ -5°C. Then the precooled gas is expanded by the JT-valve to around 3 MPa. The expansion cooling is, due to the small flow rate, performed with help of a JT-valve instead of a turbine expander. During this isenthalpic expansion, the gas is cooled to around -50°C[5] and sent into the induction section (see Figure 1) where droplets are formed.

Induction Section. The induction section is a well insulated pipe, which has a variable volume. Part of the section can be replaced, to vary both the residence time and the internal wall surface to gas volume ratio. Both variations can be accomplished by changing the inside diameter of insulated pipe. For the measurements described in this article, the residence time τ that the gas is present in the induction section has been $\tau \approx 0.3$ s. The required induction time is relevant because it determines the minimum size of well insulated semicryogenic induction section on industrial scale that is needed to deliver sufficiently sized particles to the separator, e.g., at 200 MMscf/d. A 200 MMscf/d gas treatment plant with a droplet growth time of 0.5 s already results in a requirement for $\sim$30 m of 8.5" vacuum insulated and cooled piping. This increases the costs of the system. First, compactness is required for off-shore applications. Second, we wish to minimize the length of cryogenically cooled induction pipe. Because of the slow increase in droplet size, a separator that can efficiently collect micron-sized particles is indispensable, otherwise, this would lead to very large and expensive equipment. On the small scale present in this experimental unit, a cyclone separator would be possible. Actually, the preseparator cyclone in our setup already collects most of the liquid. But on a field scale, this will not be feasible, and therefore, we make use of the rotational particle separator for field applications.

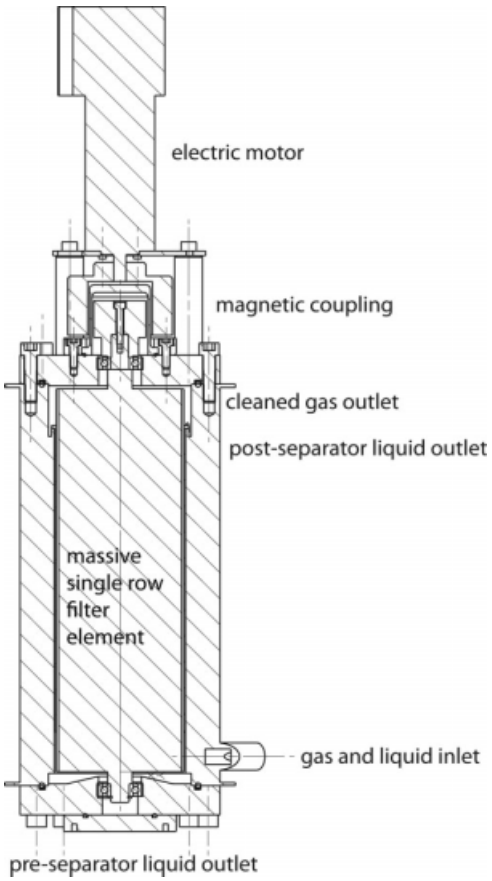

Figure 6. Rotating particle separator section-view.

The Separator. The separator consists of a motor driven coagulation element combined with a pre and postseparator (see also section Separation). The element is driven by a DC motor that is connected via a magnetic coupling. The magnetic coupling consists out of a master and slave magnet separated by a PEEK cap that provides the gas seal.

The two phase gas stream is accelerated through a tangential inlet into the preseparator as discussed in section Separation (See Figure 6). The preseparator is the zone of the separator where the coarse droplets are separated by the tangential velocity of the gas analogous to a cyclone separator. The coarse droplets collide with the wall and flow in a

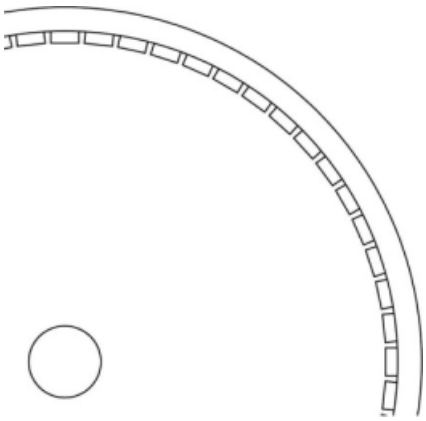

Figure 7. Cross section of the solid coagulation element.

The channels are milled in a solid duplex cylinder. The outside sleeve was shrunk around the cooled cylinder.

downward direction by gravity and are subsequently drained at the bottom side of the separator.[18] Because of the small scale of this particular separator, the preseparator zone separates already micron-sized droplets as discussed earlier. The small size is also the reason why the rotating element consists of only a single row of coagulation channels to prevent flow circulation.

Within the separator, the droplets are spatially separated from the upward flowing carrier gas, which is enriched in methane. As shown in Figure 7, the separator is constructed with a single row of milled channels around the circumference of a solid Duplex steel cylinder. The outside of the channels is constructed by combining a heated shrink sleeve and the cooled element which merge together. Within the single row of small channels, the centrifugal force, forces the droplets to the outer walls of the coagulation element.

The droplets merge into a thin film on the inside of the shrink sleeve and depending on the gas flow velocity the film is expelled at the top or bottom side of the element. The liquid that is expelled at the bottom side is drained together with the liquid from the preseparator and the liquid expelled from the top side is drained with help of a special flood groove.

Peripheral. Most of the equipment within the gas loop is only peripheral to ensure continuous recycling of the components. The incoming compressed gas flow is precooled within the evaporator, before the JT-valve expansion, with help of the separated liquid CO_2 that is evaporated.

After separation, the clean or product gas stream is heated and sent back to the gas conditioning section. The liquid CO_2 streams (or waste streams) leaving the separator are both fed to a collection vessel, which is also used for overnight CO_2 storage. To compensate for the pressure difference over the rotating element a dip-pipe is used within the collection vessel, see Figure 8.

There are two gas bypass lines, the gas bypass start-up and the gas bypass steady state. The gas bypass start-up is used to precool the evaporator and thus the incoming gas during start-up, in order to diminish start-up time. The gas bypass steady state is used to enhance the liquid drainage from the separator during the measurements. The gas flow through this bypass line lowers the pressure within the collection vessel and prevents liquid hold up in the separator.

Detection

Pressure gauges are mounted all over the setup. Temperatures are measured by thermocouples. Mass flows are measured with coriolis flow meters with an estimated error of $<\pm 5\%$. Several other flows are controlled by mass flow controllers. The liquid levels in both the evaporator and liquid collection vessel are measured by radar level meters (Endress + Hauser).

To get a reliable thermodynamic measurement, the system should be in steady state for about 1 h due to the cycle time (± 20 min) of the liquid CO_2. To get into a steady state, the system first has to run and cool down for a couple of hours to collect enough liquid CO_2. During the steady state, the concentration, temperatures, pressures, flows and liquid levels will remain constant. All presented thermodynamic measurements are performed while in steady state.

There are three main sources of errors in these measurements: loop stability, flow meters, and concentration analyzer. The errors in the temperature and pressure measurements are very small. The error in the temperature measurements is on the order of ± 0.2°C. The error in the pressure is about ± 0.001 MPa. Accuracy of the flow meters is $\pm 5\%$, and of the gas chromatograph is 1–2 mol %.

Gas concentrations of feed, product, waste, and bypass (F,P,W,B) are monitored with a four channel PPQ gas chromatograph (for sampling positions, see Figure 5). With the four channel gas chromatograph, all streams i.e., the feed,

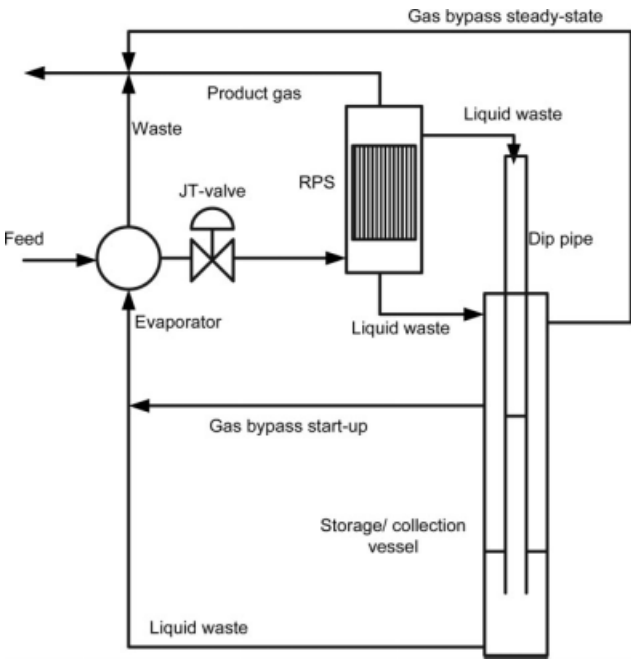

Figure 8. Detailed liquid collection, with collection vessel and bypass lines.

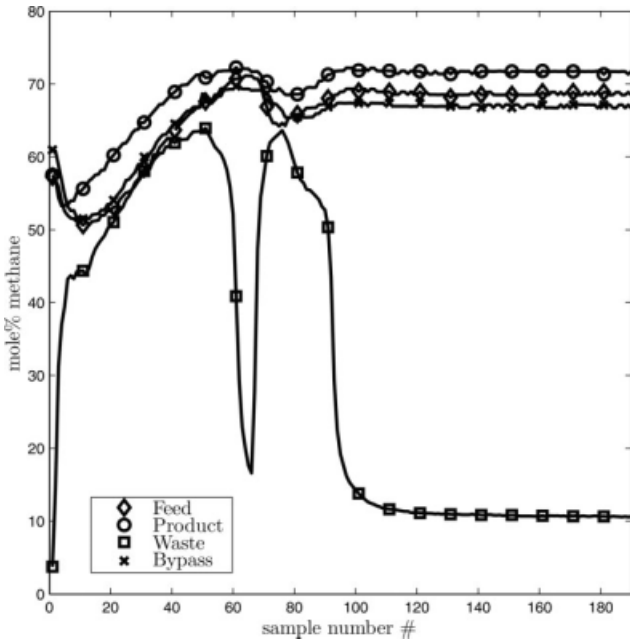

Figure 9. Simultaneous measurement of feed, product, waste, and bypass concentration via gas-chromatography (sample time ≈ 1.5 min).

Operating pressure 3.2 MPa absolute and temperature −48°C.

product, waste, and bypass can be sampled continuously with a sample time of ∼1.5 min. Although the sampling lines are kept as small as possible, due to system delays (e.g., the liquid holdup in the liquid collection vessel), the various concentrations (F,P,W,B) cannot be compared at a single time. So, we need long-duration steady-state operation to get reliable measurements. Some insight into the dynamic behavior can be gained by considering and compensating for the fluid hold up, velocities of the fluids, and mixing during storage in the collection vessel. The liquid hold up time normally exceeds 20 min. Therefore, a reliable measurement can only be performed during a steady state of more than 1h. The time needed for a reliable measurement depends on the system stability, the liquid level in the collection vessel, and several mass flow rates.

The GC consists out of four thermally conditioned PPQ columns filled with a packing suited for methane/carbon dioxide discrimination. The retention times for both gases differ by a few seconds. Helium is used as a carrier gas, which is supplied at a constant flow rate and pressure. The sample is injected into the column by an intermittent injector. The conversion into concentrations can again be calibrated with help of the premixed bottles. The device is calibrated using premixed bottles with a methane concentration of ∼0, 25, 50, 75, and 100 mol%.

Results and Discussion

When performing a measurement (see Appendix), the unit should be in ''steady state'' to eliminate the fluctuations, which result from the separation loop. The gas that is separated from the liquid droplets, is fed back to the compressor much faster than the liquid CO_2, which remains a relatively long time within the liquid collection vessel (see Figure 8). The long-time delay to measurement arises from CO_2 liquid hold up. The density of the liquid CO_2 is much higher than the density of the gas and the volume of liquid path is much larger due to the collection vessel. The cycle time of the liquid CO_2 can be more than 20 min, which results in a waiting time of more than 1 h to achieve steady state. At start-up, liquid CO_2 is collected in the liquid collection vessel to be sure that there is a liquid lock present during steady-state operation. This liquid lock is needed to prevent bypass gas from contaminating the liquid CO_2.

A typical concentration log measured via the GC can be found in Figure 9.

The figure shows a continuous concentration plot for all four streams simultaneously. The four lines represent the methane concentration mol % of the feed, product, bypass, and waste stream. The first 50 sample numbers are during start-up and cooling phase where liquid CO_2 is collected in the liquid collection vessel. When enough liquid is collected and the setup is cooled, the gas bypass steady-state (see Figure 5 and 8) is opened and the gas bypass start-up is closed, which is the transition. After the transition, it takes over an hour to get into steady state. Steady state is reached when gas concentrations, pressures, temperatures, liquid levels, and mass flow rates are all stable. In Figure 9, a downward spike in waste concentration is recorded that represents an aborted transition, which has not led to a steady state. The second transition around sample number 80 has been performed successfully. After sample number 160, the system has reached steady state. The graph shows a stable feed concentration of 68% methane, a product concentration of 72% and a liquid waste stream which consists out of 11% methane. The bypass concentration is close to the feed concentration.

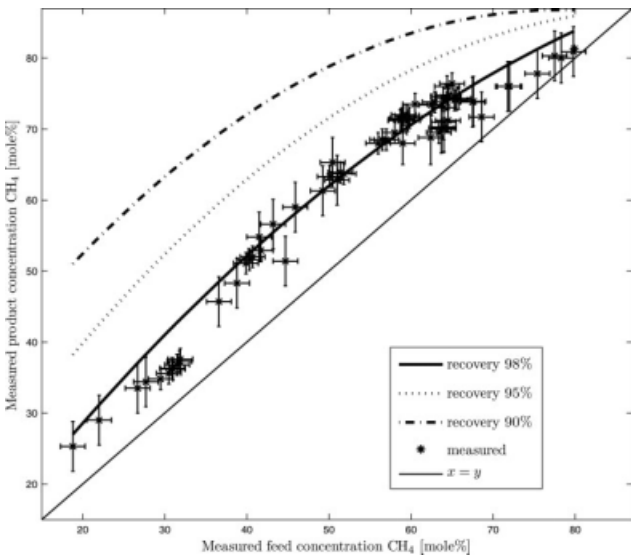

Figure 10. Measured product concentration vs. measured feed concentration.

The line $x = y$ is plotted to guide the eye. The three plotted curves are the theoretical maximum achievable enrichment for a stated recovery rate.

Because of the relatively high temperature, only a small increase in methane concentration is measured. Theoretical flash calculations at the operating pressure and temperature predict a product concentration of 72%, which is in agreement with the measurements. At the measuring conditions, 99% of the methane present in the feed stream is recovered in the product stream.

Figure 10 shows the results taken from a number of runs such as that shown in Figure 9. The measured product concentration of methane y_1 is plotted as function of the measured feed concentration of methane z_1, and these measurements have been done at several pressures and temperatures varied independently. The 45° line represents a product concentration y_1 equal to the feed concentration z_1 ($z_1 = y_1$), which is equal to no enrichment and 100% recovery.

The plotted points represent the product concentration y_1 for several measured feed concentrations z_1 at various pressures and temperatures. The error bars reflect the stability of the steady state during measurement and the analyzer reproducibility.

Because of the operating limitations of the loop (see Figure 3) only a shallow penetration of the phase diagram can be accomplished, i.e., the conditions after expansion are still close to the dew-point line. Because of the shallow penetration of the phase diagram, all measurements have been performed at low enrichment and high recovery conditions. Because of the pressure and temperature limitations of the test setup (mainly due to the compressor pressure ratio and small scale expansion), the operation window is limited. One of these limitations is the isenthalpic expansion over the JT-valve, which results in less cooling for a certain pressure drop than the isentropic cooling via a turbine expander. The pressure in the separation section may be varied between 2.5 and 3.5 MPa, and this in combination with the isenthalpic expansion limits the operating window (see Figure 3). The operation window is constrained in vertical direction between the minimal and maximal operating pressure of the loop. In the horizontal direction, the operation is limited between the dew-point line and the isenthalpic expansion curve corresponding to the JT-valve, (See Figure 3). The measurements that are presented in this article are therefore mainly done at pressures and temperatures that are nonoptimal for highest enrichment at maximum recovery. Operation can only be performed in a small area of the phase diagram located in the lower right of the two phase envelope. This limited operation window is an artefact of the loop construction. In practice, this means that operation with this test rig is limited to high-recovery and low enrichment conditions. Because these limitations are present, we can only validate model predictions at nonoptimal conditions. Because of the shallow penetration of the phase diagram, all measurements have been performed at low enrichment and high recovery conditions.

The plotted lines for $r_1 = 0.9$, $r_1 = 0.95$, and $r_1 = 0.98$ recovery are theoretical maximum achievable enrichments for these stated recovery rates with a limitation by the maximum initial pressure before expansion (van Wissen[5]). Note that the measurements do not and should not relate to any of the plotted recovery lines directly because they are performed at different pressures and temperatures. These lines represent theoretical maximum achievable enrichments for a stated recovery rate (Eq. 1) in combination with the prior stated restrictions. This predicted optimal performance cannot be validated with the current test loop due to the stated pressure and temperature restrictions. The recoveries corresponding to the presented measurements vary between 93 and 100%.

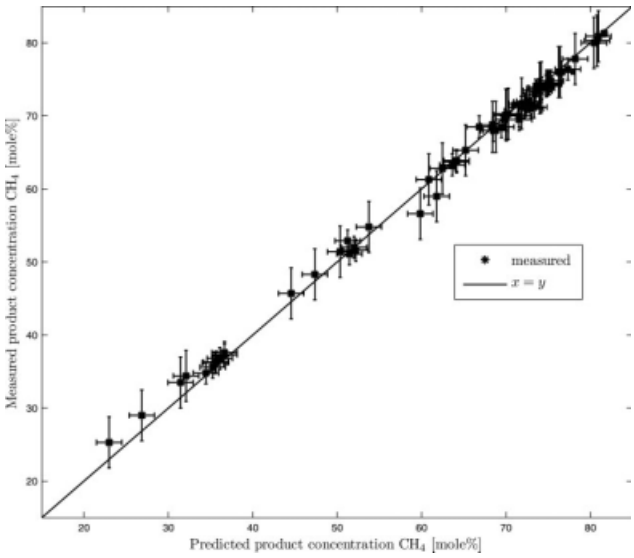

Figure 11. Comparison between the predicted and measured concentrations.

The separation performance is determined by the gas analyzer. When in a stable steady state, the rotational velocity of the separator is changed, then the change in concentration, mass flow rates, and pressures are monitored. Because of the small scale of the separator, rotational variations have a limited effect on the already high separation efficiency. This is exemplified by the high efficiency of the preseparator even at static conditions. In the case of high rotational velocities, the separation efficiency gets worse because of the additional power supplied to the element and to the small gas stream thereby increasing the temperature and the evaporation of liquid carbon dioxide. To achieve good separation, a bypass line was needed to enhance the liquid drainage from the separator. Therefore, special care should be given to the design of the liquid removal from future separators.

Because of the small flow rates (50 kscf/d) in the test-loop, it is fairly easy to separate micron-sized droplets. However, at full scale this will be one of the major challenges due to the decreasing performance at larger scales at constant energy consumption.[9]

In Figure 11, a comparison is made between the predicted and observed product concentrations (y_1) corresponding to a measured feed concentrations (z_1) shown in Figure 10.

As can be seen, the predictions and measurements are in good agreement. Because the theory and measurements agree well, one can conclude that the two phases are separated almost completely. So preferential condensation and subsequent centrifugal separation of the condensed phase is possible. To measure at conditions leading to maximum enrichment, a different test rig is required. This rig should

be built at a larger scale to incorporate the centrifugal separation testing. The enrichments and recoveries presented in this article are representative for the real, once through process, and are in good agreement with the thermodynamic predictions. Therefore, one can conclude that when complete separation of the condensed phase is achieved on full scale, the predicted performance will be achieved.

There is an intrinsic trade-off between enrichment and recovery more commonly seen in chemical processes as selectivity vs. conversion. An economical solution is to optimize the process for high enrichment up to a product gas purity of $y_1 = 0.85$ to 0.9 in one step. According to simulations, this is possible for methane concentrations in the range of $z_1 = 0.3$ to 0.9. The liquid waste then still contains a considerable amount of methane. We then apply a waste regeneration step by flashing the methane at a lower pressure and higher temperature. Liquid CO_2 can be produced with a purity of more than 95%, whereas the regenerated methane can be mixed with the contaminated gas entering the process. The produced methane still needs after treatment with a relatively small absorption unit to comply with pipeline specifications mentioned earlier.

Conclusions

1. In this article, we have demonstrated for the first time that condensed contaminant centrifugal separation (C3sep) can be used to clean contaminated natural gas containing large quantities of CO_2. The process combines expansive cooling along with a novel rotational particle separator (RPS). Use is made of the preferential condensation of CO_2 and subsequent mechanical separation of the condensed phase.

2. The unique advantage of this device is that it can remove much smaller droplets (ca. 1 μm) compared with other mechanical rotational separations such as cyclones (20 μm). In a process requiring cooled conditions, this means that separations are effected after much shorter residence times with accordingly much shorter lengths of cooled pressurised piping. This significantly cuts capital costs.

3. In this demonstration test, only a limited region of the phase diagram could be accessed because we were operating with a test loop rather than a once through system as would be the case under field conditions. The smaller scale (50 kscf/d) compared with field conditions (1000 MMscf/d) meant that a Joule-Thomson valve had to be used rather than a turbine expander. In the latter case, more effective cooling will be achieved and there will also be energy recovery for application in any subsequent compression.

4. The theoretically predicted thermodynamic equilibrium separations are achieved.

5. Once the CO_2 droplets have been collected as bulk liquid, a number of liquid drainage issues require special attention. Liquid hold up can suppress efficiency due to the changes in pressure drop across the RPS device and between the liquid and gas streams. Although primarily an artefact of the loop system tested, this will also be a feature of a once through system.

6. In this system, for safety reasons, we have only tested natural gas contaminated with CO_2. However, the same separation principles apply for natural gas contaminated with H_2S. Indeed more efficient separations should be achievable using somewhat lower temperature conditions (e.g., -90 °C), which is possible because of the much lower solid line in the corresponding phase diagram.

7. The process is a good bulk separator of natural gas contaminants; however, a tail gas treater such as an amine unit will always be required for the last few percent of contaminant to bring the gas up to pipeline specifications, i.e., 2–3%CO_2.

8. The separated waste stream is produced as a liquid, which is convenient for pumping/reinjection for carbon storage. (By contrast, a classical amine treater produces CO_2 as a low pressure gas which requires expensive recompression before sequestration.)

9. Further development of this technology will, for the reasons identified earlier , be focussed on larger scale once through processes using slip streams from field gas reservoir facilities.

Literature Cited

1. Kohl AL, Nielsen RB. *Gas Purification*, 5th ed. Houston, TX: Gulf Professional Publishing, 1997.
2. Foss MM. Interstate natural gas-quality specifications and interchangeability. www.beg.utexas.edu/energyecon/Ing, Sugar Land, TX: Center for Energy Economics. 2004;1–52.
3. Golombok M, Nikolic D. Assessing contaminated gas. *Hart's E & P Mag*. 2008; June: 73–75.
4. Brouwers JJH, van Wissen RJE, Golombok M. Novel centrifugal process removes gas contaminants, *Oil Gas J*. 2006;104:37–41.
5. van Wissen RJE. *Centrifugal Separation for Cleaning Well Gas Streams: From Concept to Prototype,* PhD thesis, Eindhoven University of Technology, 2006.
6. Younger AH. *Natural Gas Processing Principles and Technology—Part 2*. Tulsa, Oklahoma: Gas Processors Association, 2004.
7. Perry RH. *Perry's Chemical Engineers' Handbook*, 7th ed. New York: McGraw-Hill, 1999.
8. Brouwers JJH. Phase separation in centrifugal fields with emphasis on the rotational separator. *Exp Therm Fluid Sci*. 2002;26: 325–334.
9. van Wissen RJE, Brouwers JJH, Golombok M. In-line centrifugal separation of dispersed phases. *AIChE J*. 2007;53:374–380.
10. Brouwers JJH. Particle collection effciency of the rotational particle separator. *Powder Technol*. 1997;92:89–99.
11. Brouwers JJH. Rotierende partikelabscheider als neues verfahren fr die abscheidung von feinstaub und nebel aus gasen. *Chem Ingen Techn*. 1995;67:994–997.
12. Brouwers JJH. Secondary flows and particle centrifugation in slightly tilted rotating pipes. *Appl Sci Res*. 1995;55:95–105.
13. Brouwers JJH. Rotational particle separator: A new method for separating fine particles and mists from gases. *Chem Eng Technol*. 1996;19:1–10.
14. Fuchs NA. *The Mechanics of Aerosols*. Oxford: Pergamon Press, 1964.
15. Hinds WC. *Aerosol Technology*. New York: John Wiley & Sons, 1999.
16. Kuerten JGM, van Esch BPM, van Kemenade HP, Brouwers JJH. The effect of turbulence on the effciency of the rotational phase separator. *Int J Heat Fluid Flow*. 2007;28:630–637.
17. van Esch BPM, Kuerten JGM. Direct numerical simulation of the motion of particles in rotating pipe flow. *J Turbulence*. 2008;9(4):1–17.
18. Willems GP, van Esch BPM, Brouwers JJH, Golombok M. Creeping film model for condensed centrifugal separation processes. *Chem Eng Sci*. 2008;63:3358–3365.

Appendix

Table A1. Measurement Data Averaged in Three Categories: 18–40 [mol% CH_4] (14 data sets), 40–60 [mol% CH_4] (24 data sets), and 60–80 [mol% CH_4] (31 data sets)

Feed conc. range (z_1) [mol% CH_4]	Averaged feed conc. (z_1) [mol% CH_4]	Averaged product conc. (y_1)[mol% CH_4]	Averaged waste conc. (x_1)[mol% CH_4]	Averaged pressure induc. sec. [MPa, rel]	Averaged T induc. sec. [°C]	Predicted averaged product conc. (y_1) [mol% CH_4]	Predicted averaged waste conc. (x_1) [mol% CH_4]	Predicted averaged product fraction	Averaged bypass % of feed	Averaged recovery (r_1)	Averaged feed flow rate [kg/h]	Averaged product flow rate [kg/h]
18–40	30.5	37.3	6.6	2.5	−27.6	36.2	4.2	0.82	17.1	0.95	72.3	44.9
40–60	51.8	63.8	10.8	2.8	−44.2	64.1	8.9	0.78	10.2	0.95	69.3	41.0
60–80	67.0	74.1	12.4	2.9	−52.6	74.7	11.7	0.88	9.1	0.98	65.4	47.0

Manuscript received Apr. 15, 2009, and revision received June 5, 2009.